Title

Functional adaptation of interradicular alveolar bone to reduced chewing loads on dentoalveolar joints in rats

Journal

Dental Materials, 37(3)

ISSN

0109-5641

Authors

Jang, Andrew
Wang, Bo
Ustriyana, Putu
et al.

Publication Date

2021-03-01

DOI

10.1016/j.dental.2020.12.003

Peer reviewed

HHS Public Access

Author manuscript

Dent Mater. Author manuscript; available in PMC 2022 March 01.

Published in final edited form as:

Dent Mater. 2021 March ; 37(3): 486–495. doi:10.1016/j.dental.2020.12.003.

Functional adaptation of interradicular alveolar bone to reduced chewing loads on dentoalveolar joints in rats

Andrew Jang[a], **Bo Wang**[a], **Putu Ustriyana**[a], **Stuart A. Gansky**[c], **Igor Maslenikov**[d], **Alex Useinov**[d], **Richard Prevost**[e], **Sunita P. Ho**[a,b,*]

[a]Division of Preclinical Education, Biomaterials & Engineering, Department of Preventive and Restorative Dental Sciences, University of California San Francisco, CA 94143, United States

[b]Department of Urology, University of California San Francisco, CA 94143, United States

[c]Division of Oral Epidemiology & Dental Public Health, Department of Preventive and Restorative Dental Sciences, University of California San Francisco, CA 94143, United States

[d]Technological Institute of Superhard and New Carbon Materials (TISNUM), ul. Tsentral'naya 7, Troitsk, Moscow, 142190, Russia

[e]LaVision Inc. 211 W. Michigan Ave./Suite 100, Ypsilanti, MI 48197, United States

Abstract

Objectives.—The effects of reduced chewing loads on load bearing integrity of interradicular bone (IB) within dentoalveolar joints (DAJ) in rats were investigated.

Methods.—Four-week-old Sprague Dawley rats (N = 60) were divided into two groups; rats were either fed normal food, which is hard-pellet food (HF) (N = 30), or soft-powdered chow (SF) (N = 30). Biomechanical testing of intact DAJs and mapping of the resulting mechanical strains within IBs from 8- through 24-week-old rats fed HF or SF were performed. Tension- and compression-based mechanical strain profiles were mapped by correlating digital volumes ofIBs at no load with the same IBs under load. Heterogeneity within IB was identified by mapping cement lines and TRAP-positive multinucleated cells using histology, and mechanical properties using nanoindentation technique.

Results.—Significantly decreased interradicular functional space, IB volume fraction, and elastic modulus of IB in the SF group compared with the HF group were observed, and these trends varied with an increase in age. The elastic modulus values illustrated significant heterogeneity within IB from HF or SF groups. Both compression- and tension-based strains were localized at the coronal portion of the IB and the variation in strain profiles complemented the observed material heterogeneity using histology and nanoindentation.

[*]*Corresponding author*. sunita.ho@ucsf.edu (S.P. Ho).

Declaration of Competing Interest

The authors report no declarations of interest.

Appendix A. Supplementary data

Supplementary material related to this article can be found in the online version at doi:https://doi.org/10.1016/j.dental.2020.12.003.

Significance.—Interradicular space and IB material-related mechanoadaptations in a DAJ are optimized to meet soft food related chewing demands. Results provided insights into age-specific regulation of chewing loads as a plausible “therapeutic dose” to reverse adaptations within the periodontal complex as an attempt to regain functional competence of a dynamic DAJ.

Keywords

Dentoalveolar joint; Biomechanics; Digital volume correlation; Functional adaptation; Interradicular bone; Mechanoadaptation

1. Introduction

The interradicular bone in a dentoalveolar fibrous joint (DAJ) is a key structural component that reacts to chewing loads [1–7]. From a load-bearing and a structural mechanics perspective, with age, the interradicular space continues to be the narrowest periodontal ligament-space (PDL-space) between the interradicular alveolar bone (IB) and tooth-furcation. Simulation studies using mechanical testing *in situ* illustrated the interradicular alveolar bone as a biomechanically active hotspot [3]. As such, periodontal tissues specific to the interradicular region conceivably experience increased mechanical stimulation and subsequent mechanoadaptation. These changes in properties at a joint- and a tissue-level over space and time will be mapped and discussed.

The oral masticatory complex including the periodontal tissues of the DAJ adapt to chewing loads [1,2,7]. However, no information related to functional PDL-space and the mechanoadaptive properties of the load-bearing IB exists to date. Mechanoadaptation of hard/mineralized tissues including the load-bearing IB of the periodontal complex is related to the dynamic crosstalk between mineral resorption and formation mechanobiological events, and resulting organic and inorganic contents [8–11]. In particular, the effect of reduced chewing loads on a DAJ was previously quantified as differences in form (interradicular functional space between the tooth and the bone) and DAJ function (increased DAJ stiffness) [12–16]. It is hypothesized that the material properties of IB are optimized with age to meet functional demands on a DAJ. To investigate function-mediated mechanoadaptation of IB, the objectives of this study were to: (1) demonstrate from a joint biomechanics perspective that the interradicular interface with the tooth serves as the focal region of compression and adapts to chewing loads; (2) differentiate form- and material property-related adaptations of the IB, specifically from experimental groups subjected to prolonged chewing of softer foods; and (3) correlate shifts in softer and harder structural components of the periodontal complex with mechanoadaptive properties of the IB (cement lines, resorption, elastic modulus, and compression and tension strain profiles).

2. Materials and methods

Definitions of terms used in this manuscript are highlighted as nomenclature within Supplemental Information.

2.1. Reduced chewing loads in rats, an animal model [15,16]

All experimental protocols were compliant and followed the guidelines of the Institutional Animal Care and Use Committee (IACUC). Male Sprague Dawley rats (N = 60; Charles River Laboratories, Inc., Willmington, MA, USA) at four weeks of age were divided into two groups and were fed one of two nutritionally equivalent foods: hard pellet food (Hard Food = HF; N = 30) or soft powdered chow (Soft Food = SF; N = 30) (PicoLab 5058, LabDiet, Deans Animal Feeds, Redwood City, CA, USA); foods differed only in hardness (i.e., the softer food was a powdered version of the harder food) [1,2,15–17]. Hemimandibles were dissected and the right hemimandible was saved for *in situ* loading, micro X-ray computed tomography, and nanoindentation, while the left hemimandible was processed for histology. Adaptations as related to biochemical and material property changes as an effect of reduced chewing loads were recorded at 8, 12, 16, 20, and 24 weeks.

2.2. Biomechanical testing in situ and micro X-ray tomography (micro XCT) [5,15,18]

Preparation of hemimandibles for biomechanical testing under wet conditions constituted loading the DAJ *in situ* by using validated loading schemes while visualizing using a micro X-ray computed tomography system [5,15,18]. Prepared specimens were loaded under wet conditions using a load compression cell (MT200CT, Deben UK Ltd, Suffolk, UK) custom-fitted to a micro-CT (Micro XCT-200, Carl Zeiss X-ray Microscopy, Pleasanton, CA, USA). Each specimen was loaded to each permutation of a peak load (5 N, 6 N, 8 N, 10 N, and 15 N) and a displacement rate (0.2, 0.5, 1.0, 1.5, 2.0 mm/min) [5]. Two separate specimens (one 8-week HF and one 8-week SF) were prepared for visualization of tooth position relative to the socket surface, and consequently DAJ biomechanics *in situ* (Supplemental Figure S1) and digital volume correlation (DVC) was subsequently performed to generate maximum and minimum principal strains equivalent to tensile and compressive strain profiles within interradicular alveolar bone [5,15,19].

2.3. Evaluation of functional space of a loaded DAJ

In this study, PDL-space under load is defined as “functional space”, and at no load is defined as “PDL-space”. Tomograms were analyzed using AVIZO (Avizo 2019.4, Thermo Fisher Scientific, Waltham, MA, USA). Segmentations of tooth and alveolar bone were calculated based on intensity cues resulting from X-ray attenuation and segmented data were used to generate surface meshes. The segmented data were checked manually to confirm accurate extraction of morphological features. The net PDL-space was calculated by subtracting PDL-space under load and from PDL-space under unloaded conditions. The resulting net PDL-space was mapped on the tooth surface.

2.4. Mapping tartrate-resistant acid phosphatase positive (TRAP)(+) regions within a complex [20,21]

Left hemimandibles were fixed, decalcified, and embedded in paraffin as previously described [20,22]. TRAP staining for osteoclastic activity was performed and tissue sections were counterstained using hematoxylin. Individual multinucleated cells in the distal periodontal complex and within the interradicular alveolar bone displaying a TRAP(+)

response were counted. Statistically significant differences between HF and SF groups were calculated for each age group using Student's t-test.

2.5. Nanoindentation and bone volume fraction (BVF) of interradicular bone [23–25]

Hemimandibles (N = 3 for each age group from respective SF or HF groups) were prepared for nanoindentation by polishing using silicon carbide grit and diamond slurries of various grades (Buehler Ltd., IL, USA) [26]. The polished specimens were immobilized for nanoindentation using epoxy and care was taken to avoid its infiltration into the specimen. Nanoindentation (Nanoscan 4D, Nanounity, Moscow, Russia) on polished surfaces was performed under wet conditions using a Berkovich tip. On average, 20–25 indents were made using 2000 μN load and each indent was placed 16 μm apart on the IB and specifically in regions that were in direct association with the second molar. Reduced elastic modulus (Er) [23] was calculated and elastic modulus by age and by food hardness was skewed, so a nonparametric test of age × food hardness, overall food hardness, overall age, and age-specific food hardness effects was performed with stepdown Šidák tests to correct for multiple comparisons. Statistical analyses were performed with SAS version 9.4 (SAS Institute, Inc., Cary, NC, USA).

Bone volume fraction (BVF) was calculated using subvolumes within three-dimensional volumes reconstructed from X-ray tomograms [24,25]. Statistically significant differences between harder and softer foods were calculated for each age group using the Student's t-test.

2.6. Image processing and digital volume correlation to map maximum and minimum principal strains in interradicular alveolar bone [5,19]

Strain mapping of an interradicular alveolar bone under load was performed on a single specimen from each group (8 weeks only). Piecewise DVC was performed to compare deformations between 0–7 N, 7–15 N, and 15–20 N load configurations (DaVis software, LaVision Inc., Ypsilanti, MI, USA). The specimens were loaded at rate of 2 mm/min. Maximum and minimum principal strains equivalent to tensile and compressive strains within interradicular alveolar bone [5,15,19] were evaluated and mapped.

Prior to digitally correlating the volumes of interradicular bones at no load and under load, all X-ray tomograms were filtered, registered, and masked. After reconstruction of the volumes, 3D images were further processed to optimize the calculation of strains by filtering, rigid body registration, cropping, and masking. Firstly, X-ray tomograms were filtered using an anisotropic diffusion algorithm within Avizo (Avizo 8.1.0, FEI, Germany) to remove 'salt and pepper' noise while preserving features. Secondly, scans acquired under loaded and unloaded conditions were used to track rigid body movement. Cropping was performed to focus on regions of interest and remove extraneous regions that would add noise (such as the beam hardening of the anvil). Finally, the tooth was removed digitally by masking away the regions of tooth structure from the image space using an intensity segmentation method. In DVC software, correlation between unloaded and loaded scans was performed by setting the interrogation window size at 64 pixels with a 50% overlap and a 25% minimum fraction of valid pixel (mvfp) [19]. The noise floor for DVC and calculation

to obtain maximum and minimum normal strains are shown in Supplemental Figures S2 and S3(a), respectively.

2.7. Statistical modeling and overall significance

Nonlinear quadratic mixed effects regression models with normal random animal × replicate effects were used for each of 125 combinations of age × force × displacement rate to model the relationship of displacement on load (load-displacement curve) between foods of two different hardness values (HF, SF) with a 3-degree-of-freedom (3 d.f.) test of the food hardness difference parameters (intercept, linear slope, and quadratic slope). These models were also used to predict the difference between food hardness in displacement to yield 5 N, 10 N, and 15 N loads as

$$\begin{aligned} &\hat{dis}p_S - \hat{dis}p_H \\ &= \frac{-\left(\hat{b}_1 + \hat{g}_1\right) + \sqrt{\left(\hat{b}_1 + \hat{g}_1\right)^2 - 4\left(\hat{b}_2 + \hat{g}_2\right)\left(\hat{b}_0 + \hat{g}_0 - load\right)}}{2\left(\hat{b}_2 + \hat{g}_2\right)} \\ &- \frac{-\hat{b}_1 + \sqrt{\hat{b}_1^2 - 4\hat{b}_2\left(\hat{b}_0 - load\right)}}{2\hat{b}_2}, \end{aligned}$$

where b_0 is the intercept for hard food, b_1 is the linear slope for hard food, b_2 is the quadratic slope for hard food, g_0 is the intercept difference from soft food, g_1 is the difference in linear slope from soft food, g_2 is the difference in quadratic slope from soft food, and *load* is 5, 10, or 15 N.

3. Results

3.1. Changes in tooth and bone association during loading in situ

A load-displacement curve highlighting plausible reactionary forces from various tissue contributions is shown in Fig. 1(a) and corresponding tooth association with alveolar bone can be seen in respective virtual sections. By tracking the tooth movement within the socket, functional space was measured (that is, PDL-space when under load) showing that the reduction in PDL-space is greatest, which means that the functional space around the interradicular alveolar bony crest is the least (Fig. 1b, center). The functional-space distribution highlighting both widened and narrowed regions within the periodontal complex of a loaded DAJ is shown relative to the uniform distribution of PDL-space within the periodontal complex of an unloaded DAJ (Fig. 1b, right). Additionally, deformation within alveolar bone was visible within the interradicular regions (Fig. 1a and Supplemental Figure S1). Statistically significant differences in stiffness values of respective tissues of the DAJs subjected to respective food hardnesses were seen from the 3 d.f. quadratic model tests of the load-displacement curves in the vast majority (116 or 93%) of the 125 age × peak load – displacement rate combinations (Fig. 1c).

3.2. Bone volume fraction and osteoclastic activity in the interradicular bone

The distribution of TRAP(+) cells within the regions of interest are shown in Fig. 2(a). Quantitative analysis of number of TRAP(+) cells was performed on preferentially localized

cells in the distal region within all specimens regardless of age or food hardness. Within the distal region of the root, TRAP(+) cell counts were significantly greater in the HF group compared to the SF group at 8 and 16 weeks of age ($p < 0.05$). The number of TRAP(+) cells decreased with an increase in age regardless of HF or SF groups. There was little to no presence of TRAP(+) cellular activity within IB, a finding that did not change with age or food hardness. In the interradicular region of both food hardness groups, counterstaining of tissue sections with hematoxylin revealed cement lines and a large number of osteons more in the hard food group, indicating an active remodeling process.

3.3. Elastic modulus of the interradicular alveolar bone

The region of interest for the nanoindentation experiment and the histogram distributions of elastic modulus values from nanoindentation are shown in Fig. 2(b and c), respectively. For elastic modulus of interradicular alveolar bone, the nonparametric age × food hardness interaction effect was statistically significant ($p < 0.001$), indicating that the food hardness effect differed between the age groups. Weeks 12 and 24 were selected to be correlated with groups without and with statistical differences in BVF. At 12 weeks, the elastic modulus of interradicular alveolar bone within the HF (14 ± 7 GPa) was significantly greater than that of SF (10 ± 4 GPa). However, at 24 weeks, the elastic modulus of HF decreased and converged with that of SF groups and did not show a significant difference between groups.

3.4. Bone volume fraction and strain distribution within interradicular bone in response to simulated loading

Regions of alveolar bone highlighting the interradicular portion for BVF and DVC are shown in Fig. 3 (a) (left). Regions segmented into either interradicular alveolar bone or intertrabecular space in both HF (red) and SF (blue) groups are also shown in Fig. 3(a) (center). Changes in BVF were observed as a function of age and food hardness (Fig. 3a, right). BVF increased with age regardless of food hardness. There is no significant difference in BVF values between HF and SF groups at 8–20 weeks. At 24 weeks, however, the interradicular alveolar bone from the HF group had a significantly higher BVF than that from the SF group.

The 3D maximum principal strain solutions produced from DVC of alveolar bones of 8-week-old rats in HF and SF groups are shown in Fig. 3(b and c), respectively. Additional maps of three normal strains are shown in Supplemental Figure S3(b–d). The most apparent difference between HF and SF maximum and minimum normal strain maps (Fig. 3b and 3c, Supplemental Figures S4 and S5) was seen primarily at the crest (most coronal) portion of the IB. For the maximum normal strain maps, the HF group showed increased strain at the 7–15 N and 15–20 N stages compared with SF group (Fig. 3b). Only slight differences in minimum normal strain were observed between HF and SF groups (Fig. 3c). The distributions of the maximum and minimum normal strains in different loading ranges are shown in Fig. 3(d and e), respectively. Line profiles of maximum and minimum normal strains along the coronal-apical length of IB are shown in Fig. 3(f). The graphs highlighted the maximum variation in the coronal aspect of IB, regardless of HF or SF groups, and the apparent difference in the maximum normal strains are shown as spatial maps.

4. Discussion

The objectives of this study were to: (1) demonstrate from a joint biomechanics perspective that the interradicular interface of the alveolar bone with the cementum of the tooth serves as the focal region of compression and adapts to chewing loads; (2) differentiate form- and material property-related adaptations of the IB specifically from experimental groups subjected to prolonged chewing of softer foods; and (3) correlate shifts in softer and harder structural components of the periodontal complex with mechanoadaptive properties of interradicular alveolar bone (cement lines, resorption, elastic modulus, and tensile and compressive strain profiles).

Results from these objectives related to function-mediated mechanoadaptation of the interradicular alveolar bone will be discussed at joint- and tissue-levels respectively. The observed heterogeneity in tensile and compressive strain profiles within the IB complementing the variance in intrinsic material properties of the IB will be discussed in the context of function. It is for this reason, a multiscale biomechanics approach on intact DAJ was sought to differentiate the effects of reduced chewing loads on time-related mechanoadaption of IB. It should be noted that loading rates on adapted mandibles from soft and hard food groups used in biomechanical testing *in situ* were equivalent to mastication rates of rats on softer and harder foods, respectively [1,2,27]. Simulated mastication rates included a) lower compressive loads equivalent to softer food [2,27–33] and b) higher compressive loads equivalent to harder (normal) food [2,27–33]. Based on masticatory muscle activity [17,28,30,34–39], the range of peak loads for rats on softer and harder foods is 3–6 N [29–32]. The peak loading rates for biomechanical test *in situ* varied from 5 to 30 N/s and these are only equivalent but not equal to *in vivo* loading schemes. These *in situ* loading schemes were designed to approximate stiffness of DAJs from control and experimental groups. In addition, coupling biomechanical testing *in situ* with X-ray imaging allowed visualization of tooth position relative to an alveolar socket adapted to softer and harder foods in rats under loaded conditions. As such, the steep increase in reactionary loads for a very small change in PDL-space as observed in load-displacement curves (see Supplemental Figure S1) provided additional confirmation that for peak loads over 5–7 N, increased stresses could be observed in the alveolar bone.

The effect of prolonged action of chewing loads on the DAJ was revealed by significant differences in slopes of load-displacement curves of DAJs from softer and harder food groups (Fig. 1c). Alveolar bone response to physiological or pathological loads (magnitude, frequency and direction of forces), in general, is measured through altered biochemical expressions with limited correlation to localized strains within tissues. Regardless, biochemical expressions continue to be altered until the tissues of a joint adapt both in shape and mechanical properties, a state of equilibrium necessary to sustain loads. The constitutive properties of the tissues, in particular react to loads on a joint, which could be loads equivalent to food hardness. In this study, the primary reactionary outcome of the DAJ to an external load equivalent to 7 N was observed as a nonlinear distribution of force as the tooth displaced over a few microns equivalent to the PDL-space within the alveolar socket (Fig. 1a). Increased loading greater than 7 N on the tooth could have resulted in “recording” strain stiffening of the PDL, and subsequently reactionary contribution from the harder and solid

elements including alveolar bone and tooth-related tissues (cementum, dentin, and enamel), and collagen. Conceivably, the reactionary forces are equivalent to food hardness, which primarily is the chewing load on a DAJ. It is plausible that a portion of the reactionary force specifically at lower loads can be afforded by the softer ligament, and the effect of function-mediated adaptations in the harder tissues is felt at higher peak loads (Fig. 1a).

Function-mediated adaptations in tissues resulting from prolonged loads on DAJs from SF and HF groups were correlated with osteoclastic distribution by localizing TRAP in the IB, and at the PDL-bone and PDL-cementum enthesial zones. In any given periodontal complex from the control group, TRAP(+) cells were located primarily on the distal side of the periodontal complex (Fig. 2a) and were in agreement with the distal drift process that naturally occurs in a rodent [11,12]. The reduction of osteoclasts on the distal PDL-bone interface in the SF group compared with the HF group suggests that this naturally occurring distal drift in rodents is linked to the magnitude and frequency of masticatory forces felt by cells at the respective entheses. Fewer TRAP(+) cells were observed within the interradicular crest (Fig. 2a) and could possibly serve as a mechanism for the relatively narrowed functional-space in SF group [7]. It can be argued that the lack of osteoclast activity in the SF group specifically in the IB could alter the blastic activity—a necessary crosstalk between the clastic and blastic cells to also maintain alveolar bone volume as indicated by changes in porosity resulting in a change in BVF (Fig. 3). The lack of clastic activity and the presence of cement lines in both HF and SF groups (Fig. 2a) indicates that the adaptive process leading to a shift in BVF could result from affected mineral formation-related (blastic) events. This remodeling adaptation is further complemented by the cement lines (Fig. 2a) and altered material properties (Fig. 2c).

To investigate the effect of changes in form (BVF) and material properties (elastic modulus) from a biomechanics perspective, adapted joints harvested from 8-week-old rats that illustrated a significant shift in joint stiffness (Fig. 1c) were loaded, scanned with X-rays and subsequently DVC was performed. Spatial correlation of digital volumes at no load with those at load provided an estimate of maximum and minimum principal strains within IBs of DAJ from SF and HF groups. The observed variation in strain in coronal IB using biomechanical testing *in situ* (joint-level) on intact DAJ complemented coronal IB heterogeneity (tissue-level) as identified using nanoindentation technique on specimens reduced to the sites of interest. As such, the data from the DVC is appreciated to the extent of highlighting site-specific heterogeneity (Fig. 2) in coronal aspects of the IB, that is, that which is in initial contact as the tooth moves into the socket under the conditions of simulated function (Fig. 3). An additional nuance is that the experimental biomechanics hybrid approach under *ex vivo* conditions does not account for hydrostatic pressure that results from active circulatory system [40]. The approach sought in this study is exclusive to detecting relative shifts in DAJ biomechanics *ex vivo*.

Based on the approach sought and the mapped outcome measures, temporal discretization of joint biomechanics as related to changes in individual tissues provides newer insights into spatiotemporal mechanoadaptive responses of tissues and collectively the joints. Furthermore, the effectiveness of a mechanical dose (magnitude, frequency and duration of mechanical load(s)) on a patient lies within an opportune age-dependent window.

5. Conclusions and limitations

This study highlighted spatial and temporal adaptation of IB to reduced chewing loads. Visualization of hotspots and adapted regions was enabled through a hybrid approach; functional imaging, which is a combination of X-ray imaging with biomechanics *in situ* and DVC. DVC-based results fundamentally highlighted a dominance of compression- and tension-based strains within anatomy-specific hotspots of the periodontal complex, namely, the interradicular region of the alveolar bone regardless of softer or harder foods. In line with our previous results, softer and harder tissues of the DAJ were affected by food hardness and with age but at different rates. At younger ages, tissues and interfaces of the periodontal complex of a DAJ exhibited different material properties, while significant adaptations in the alveolar bone architecture were apparent at older ages. It is probable that the load-mediated crosstalk between osteoblast and osteoclast activities is one of the multiple key factors that would alter the "quality" of alveolar bone; mechanobiological processes which are specific to anatomy (space) and, time (temporal, duration of the experiment at different ages), but reactionary to age-specific functional demands.

Based on the results from this study, a significant point to note is that, nanoindentation data should not be correlated to BVF as they are sets of data from analytical and imaging techniques that provide information at two different length scales. However, it is plausible that the effect of nanomechanical properties and BVF can be experimentally and numerically modeled through testing scenarios by using materials with the same porosity and different material properties, and vice versa, to predict the effect of their collective properties on DAJ function. On the other hand, mechanical strain within IB mapped at a tissue-level using DVC can be correlated to BVF, as it is directly affected by the architecture of bone and both parameters are acquired from imaging techniques at similar length-scales.

Multiscale biomechanics approach enabled contextualization of coronal IB heterogeneity (tissue-level) within DAJ-simulated function (joint-level). More studies, however, are warranted to delineate statistically relevant differences in mechanical strains of alveolar bones adapted to HF and SF groups. Significant advances in biomechanics *in vivo* also are warranted to gather insights into tissue-level mechanobiological time-sensitive events that otherwise would be lost when testing *ex vivo*. Systematic mapping of mechanobiological and related adaptive events, both of which can be different in space and time, can provide insights into load-related therapies with a prescribed mechanical dose to maintain the functional competence of a DAJ.

Supplementary Material

Refer to Web version on PubMed Central for supplementary material.

Acknowledgements

The authors would like to thank Ms. Grace Nonomura for her help in specimen preparation. The authors thank the Biomaterials and Bioengineering Correlative Microscopy Core (http://bbcmc.ucsf.edu), UCSF for the use of their MicroXCT-200 and biomechanical testing *in situ*.

Funding

This work was supported by the National Institutes of Health, NIDCR R01 DE022032 (SPH) and NIDCR R21 DE027138 (SPH).

REFERENCES

[1]. Hiiemae K, Heath MR, Heath G, Kazazoglu E, Murray J, Sapper D, et al. Natural bites, food consistency and feeding behaviour in man. Arch Oral Biol 1996;41:175–89. [PubMed: 8712974]

[2]. Hiiemae KM. Masticatory function in the mammals. J Dent Res 1967;46:883–93. [PubMed: 5234390]

[3]. Chattah NL, Kupczik K, Shahar R, Hublin JJ, Weiner S. Structure-function relations of primate lower incisors: a study of the deformation of Macaca mulatta dentition using electronic speckle pattern interferometry (ESPI). J Anat 2011;218:87–95. [PubMed: 20408905]

[4]. Naveh GR, Shahar R, Brumfeld V, Weiner S. Tooth movements are guided by specific contact areas between the tooth root and the jaw bone: a dynamic 3D microCT study of the rat molar. J Struct Biol 2012;177:477–83. [PubMed: 22138090]

[5]. Lin JD, Ozcoban H, Greene JP, Jang AT, Djomehri SI, Fahey KP, et al. Biomechanics of a bone-periodontal ligament-tooth fibrous joint. J Biomech 2013;46:443–9. [PubMed: 23219279]

[6]. Jang A, Chen L, Shimotake A, Landis W, Altoe V, Aloni S, et al. A force on the crown and tug of war in the periodontal complex. J Dent Res 2018;97:241–50. [PubMed: 29364757]

[7]. Jang AT, Chen L, Shimotake AR, Landis W, Altoe V, Aloni S, et al. A force on the crown and tug of war in the periodontal complex. J Dent Res 2018;97:241–50. [PubMed: 29364757]

[8]. Roberts WE, Epker BN, Burr DB, Hartsfield JK, Roberts JA. Remodeling of mineralize tissues, part II: control and pathophysiology. Semin Orthod 2006;12:238–53.

[9]. Roberts WE, Huja S, Roberts JA. Bone modeling: biomechanics, molecular mechanisms, and clinical perspectives. Semin Orthod 2004;10:123–61.

[10]. Roberts WE, Roberts JA, Epker BN, Burr DB, Hartsfiled JK Jr. Remodeling of mineralized tissues, Part I: The Frost Legacy. Semin Orthod 2006;12:216–37.

[11]. Roberts-Harry D, Sandy J. Orthodontics. Part 11: orthodontic tooth movement. Br Dent J 2004;196(391), quiz 426.

[12]. Herring SW, Pedersen SC, Huang X. Ontogeny of bone strain: the zygomatic arch in pigs. J Exp Biol 2005;208:4509–21. [PubMed: 16339870]

[13]. Hylander WL, Johnson KR. In vivo bone strain patterns in the zygomatic arch of macaques and the significance of these patterns for functional interpretations of craniofacial form. Am J Phys Anthropol 1997;102:203–32. [PubMed: 9066901]

[14]. Jang AT, Gansky SA, Maslenikov I, Rangell B, Useinov A, Prevost R, et al. Adaptation of the biomechanically active interradicular bone to reduced functional loads. Under review 2016.

[15]. Jang AT, Merkle A, Fahey K, Gansky SA, Ho SP. Multiscale biomechanical responses of adapted bone-periodontal ligament-tooth fibrous joints. Bone 2015.

[16]. Niver EL, Leong N, Greene J, Curtis D, Ryder MI, Ho SP. Reduced functional loads alter the physical characteristics of the bone-periodontal ligament-cementum complex. J Periodont Res 2011;46:730–41.

[17]. Kiliaridis S, Bresin A, Holm J, Strid KG. Effects of masticatory muscle function on bone mass in the mandible of the growing rat. Acta Anat (Basel) 1996;155:200–5. [PubMed: 8870788]

[18]. Jang AT, Lin JD, Seo Y, Etchin S, Merkle A, Fahey K, et al. In situ compressive loading and correlative noninvasive imaging of the bone-periodontal ligament-tooth fibrous joint. J Visualized Exp 2014.

[19]. Jang A, Prevost R, Ho SP. Strain mapping and correlative microscopy of the alveolar bone in a bone-periodontal ligament-tooth fibrous joint. Proc Inst Mech Eng Part H: J Eng Med 1989–1996 2016.

[20]. Leong NL, Hurng JM, Djomehri SI, Gansky SA, Ryder MI, Ho SP. Age-related adaptation of bone-PDL-tooth complex: Rattus-Norvegicus as a model system. PLoS One 2012;7:e35980. [PubMed: 22558292]

[21]. Edsall SC, Franz-Odendaal TA. A quick whole-mount staining protocol for bone deposition and resorption. Zebrafish 2010;7:275–80. [PubMed: 20807038]

[22]. Sawyer A, Lott P, Titrud J, McDonald J. Quantification of tartrate resistant acid phosphatase distribution in mouse tibiae using image analysis. Biotech Histochem 2003;78:271–8. [PubMed: 14989645]

[23]. Oliver WC, Pharr GM. An improved technique for determining hardness and elastic-modulus using load and displacement sensing indentation experiments. J Mater Res 1992;7:1564–83.

[24]. Parfitt AM, Goldstein S, Compston J. Bone quality: what is it and can we measure it? Am Soc Bone Mineral Res 2005.

[25]. Carter DR, Bouxsein ML, Marcus R. New approaches for interpreting projected bone densitometry data. J Bone Miner Res 1992;7:137–45. [PubMed: 1570758]

[26]. Ho SP, Balooch M, Marshall SJ, Marshall GW. Local properties of a functionally graded interphase between cementum and dentin. J Biomed Mater Res A 2004;70:480–9. [PubMed: 15293322]

[27]. Hiiemae K Mechanisms of food reduction, transport and deglutition: how the texture of food affects feeding behavior. J Texture Stud 2004;35:171–200.

[28]. Mavropoulos A, Ammann P, Bresin A, Kiliaridis S. Masticatory demands induce region-specific changes in mandibular bone density in growing rats. Angle Orthod 2005;75:625–30. [PubMed: 16097232]

[29]. Mavropoulos A, Bresin A, Kiliaridis S. Morphometric analysis of the mandible in growing rats with different masticatory functional demands: adaptation to an upper posterior bite block. Eur J Oral Sci 2004;112:259–66. [PubMed: 15154925]

[30]. Mavropoulos A, Kiliaridis S, Bresin A, Ammann P. Effect of different masticatory functional and mechanical demands on the structural adaptation of the mandibular alveolar bone in young growing rats. Bone 2004;35:191–7. [PubMed: 15207756]

[31]. Thomas NR, Peyton SC. An electromyographic study of mastication in the freely-moving rat. Arch Oral Biol 1983;28:939–45. [PubMed: 6580850]

[32]. Kiliaridis S Masticatory muscle function and craniofacial morphology. An experimental study in the growing rat fed a soft diet. Swed Dent J Suppl 1986;36:1–55. [PubMed: 3465055]

[33]. Niver E, Leong N, Greene J, Curtis D, Ryder MI, Ho SP. Reduced functional loads alter the physical characteristics of the bone-PDL-cementum complex. J Periodont Res 2011, under review.

[34]. Kiliaridis S, Engstrom C, Thilander B. Histochemical analysis of masticatory muscle in the growing rat after prolonged alteration in the consistency of the diet. Arch Oral Biol 1988;33:187–93. [PubMed: 3178538]

[35]. Kiliaridis S, Johansson A, Haraldson T, Omar R, Carlsson GE. Craniofacial morphology, occlusal traits, and bite force in persons with advanced occlusal tooth wear. Am J Orthod Dentofacial Orthop 1995;107:286–92. [PubMed: 7879761]

[36]. Kiliaridis S, Kjellberg H, Wenneberg B, Engstrom C. The relationship between maximal bite force, bite force endurance, and facial morphology during growth. A cross-sectional study. Acta Odontol Scand 1993;51:323–31. [PubMed: 8279273]

[37]. Kiliaridis S, Shyu BC. Isometric muscle tension generated by masseter stimulation after prolonged alteration of the consistency of the diet fed to growing rats. Arch Oral Biol 1988;33:467–72. [PubMed: 3245777]

[38]. Kiliaridis S, Tzakis MG, Carlsson GE. Effects of fatigue and chewing training on maximal bite force and endurance. Am J Orthod Dentofacial Orthop 1995;107:372–8. [PubMed: 7709901]

[39]. Odman A, Mavropoulos A, Kiliaridis S. Do masticatory functional changes influence the mandibular morphology in adult rats. Arch Oral Biol 2008;53:1149–54. [PubMed: 18721914]

[40]. Herring SW. In: Mineralized tissues in oral and craniofacial science: biological principles and clinical correlates. 1st ed; 2012.

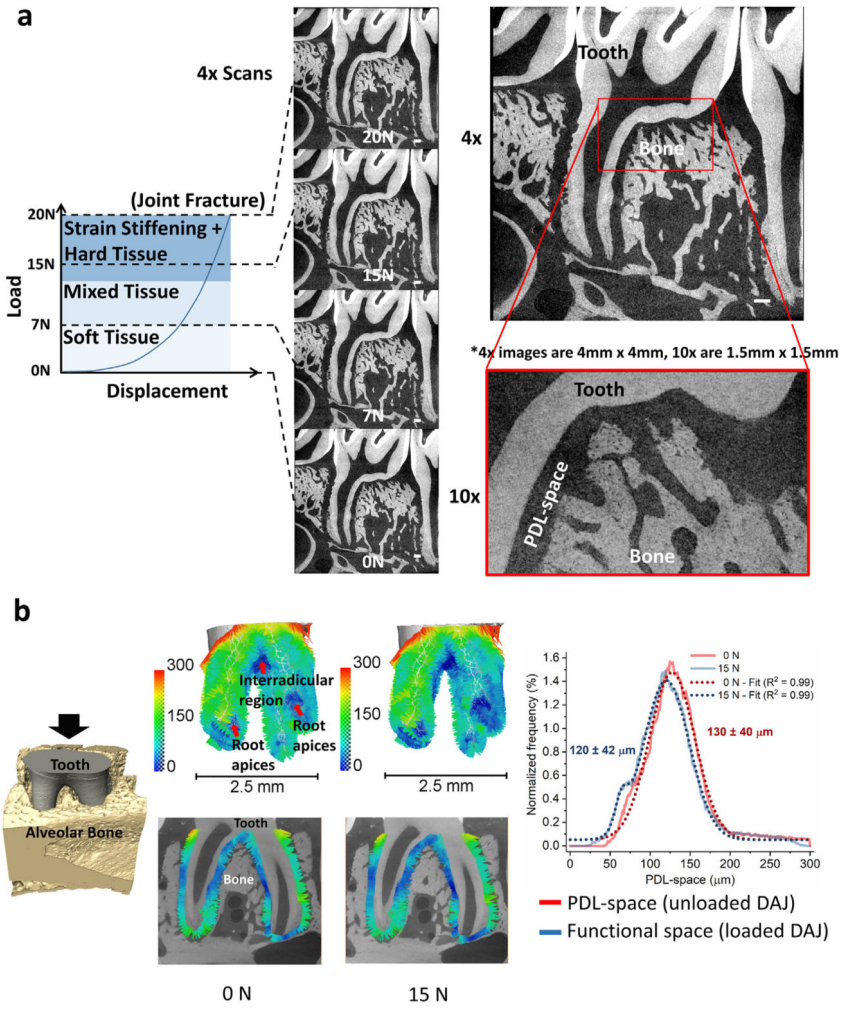

c

		Age (weeks)					
		8	12	16	20	24	all
	Force (N)	# p≤0.05	# p≤0.05	# p≤0.05	# p≤0.05	# p≤0.05	# p≤0.05
HT	15	5	5	5	5	5	25
HT	10	5	5	5	5	5	25
MT	8	5	5	4	5	5	24
ST	6	5	5	4	3	4	21
ST	5	4	5	4	4	4	21
	all	24	25	22	22	23	116

Fig. 1 –.

DAJ biomechanics, and PDL-spaces and functional-spaces of respective DAJs. (a) A representative nonlinear load-displacement curve represents plausible biomechanical events as the tooth is compressed into the alveolar socket (refer to Supplemental Figure S1 for gif animation). Identical virtual sections taken at 0 N, 7 N, 15 N and 20 N load increments illustrate tooth position relative to the alveolar socket with increasing load. White bars = 200 μm. (b) (left) The configuration of the tooth and bony socket showed the relative position of the tooth at 0 N and 15 N. (center) Tethered vectors highlight PDL-space (DAJ at no load)

and functional-space (DAJ under load) with narrowed and widened spaces within the interradicular and apical regions under simulated loading conditions. (right) Histograms illustrated PDL-space at 0 N (red) and functional-space at 15 N (blue) along with Gaussian fits (dashed red and blue lines). (c) Analyses of load-displacement curves illustrated the number (out of 5) of DAJs from soft and hard food groups that expressed stiffness values which are statistically different at 7, 15, and 20 N. HT - hard tissue; MT - mixed tissue; ST-soft tissue.

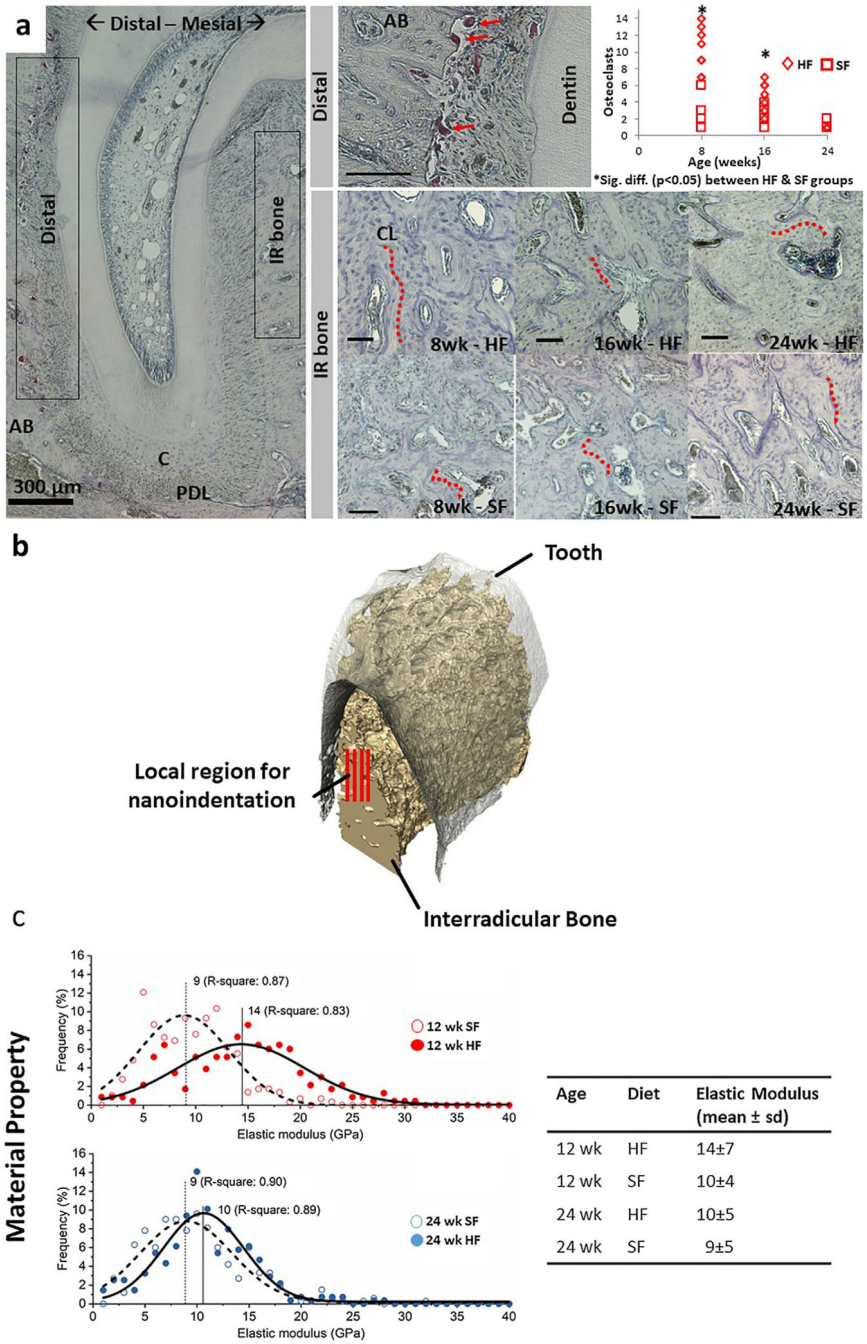

Age	Diet	Elastic Modulus (mean ± sd)
12 wk	HF	14±7
12 wk	SF	10±4
24 wk	HF	10±5
24 wk	SF	9±5

Fig. 2 –.

Interradicular alveolar bone and site-specific tissue properties. (a) Distal side of the DAJ illustrated TRAP(+) osteoclasts. Multinucleated TRAP(+)cells (red arrows) were observed at the PDL-bone enthesis. Osteoclast count along the distal edge of the periodontal complex was significantly lower ($p < 0.05$) in 8- and 16-week-old rats fed softer foods. Within the interradicular bone, cement lines (red dotted lines) indicated a footprint of combined osteoclastic and blastic activities. However, the TRAP activity within the interradicular bone region was minimal and did not vary with age or food hardness. Unless indicated otherwise,

black bars are 100 μm. (b) 3D but only a portion of the interradicular volume illustrates red lines representative of rows of nanoindentations on interradicular bone. (c) Heterogeneity in physical properties of interradicular bone (distribution, mode, and R-square) was highlighted in the form of decreased elastic modulus of alveolar bone from the SF group compared to the HF group at 12 and 24 weeks of age. The difference in mean elastic modulus values between the two groups was lower in the 24-week suggesting a converging pattern in properties across groups with an increase in age. The table shows mean elastic modulus and standard deviation of different diet groups at 12 and 24 weeks. Alveolar bone (AB), Periodontal ligament (PDL), Cementum (C), Interradicular (IR), Cement line (CL).

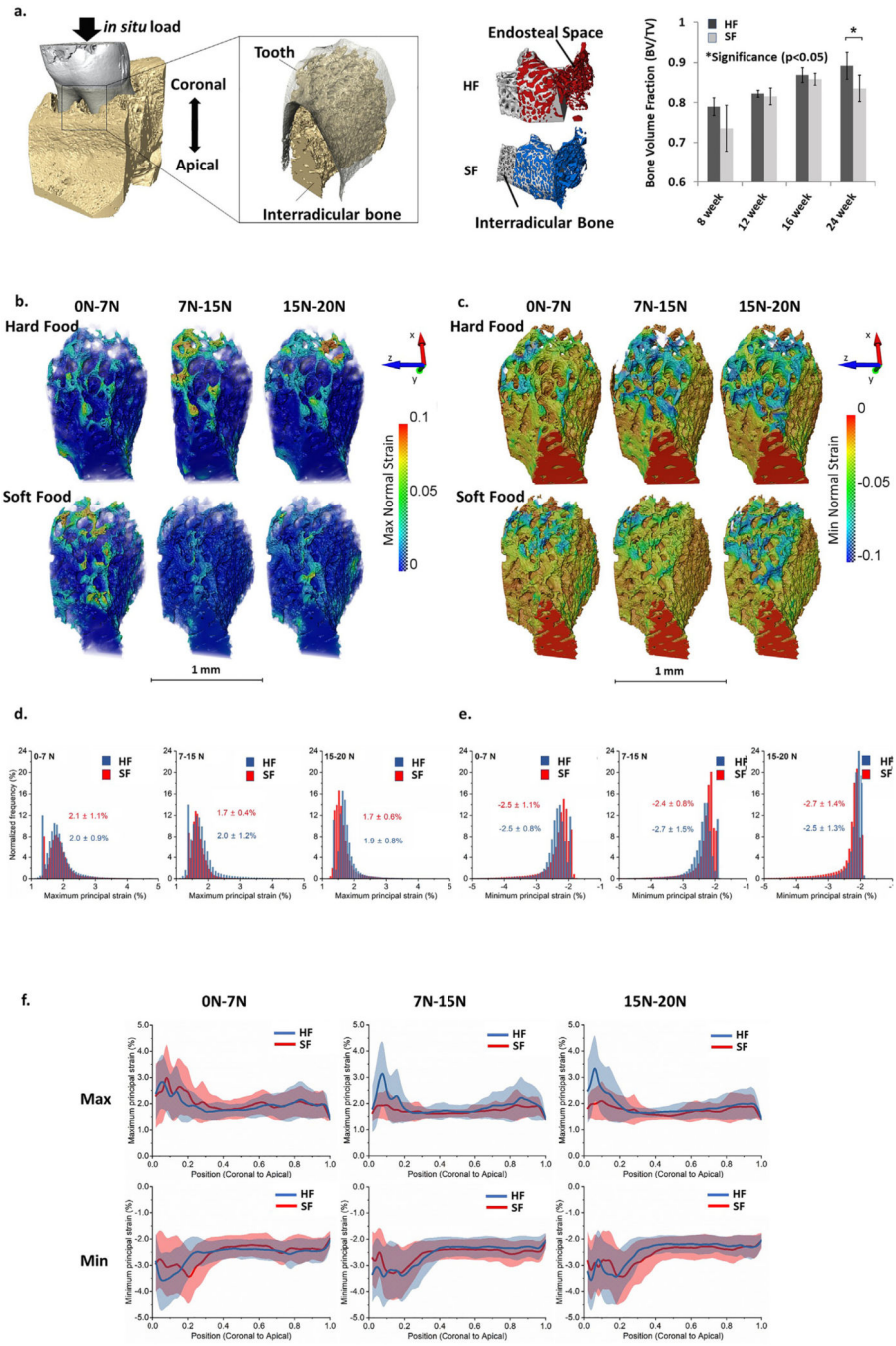

Fig. 3 –.

Tensile and compressive strain maps and line profiles of mean strain values within interradicular bone specific to hard and soft food food hardness groups. (a) (left) 3D rendered volume of a DAJ along with a segmented volume and a surface of interradicular bone are shown. (center) Differences in porosity of interradicular alveolar bone in HF (red) and SF (blue) groups were observed. (right) Adaptations in bone architecture were measured in interradicular bone by calculating bone volume fraction (BVF) from three-dimensional volumes reconstructed using X-ray tomograms. BVF of interradicular bone increased with

age and a significant difference between HF and SF groups at 24 weeks was observed. This figure is adapted with permission from Jang et al. ©2015 Elsevier. (b and c) Stepwise (7, 15, and 20 N) maximum (b) and minimum (c) normal strain maps in HF and SF groups to represent the incremental strain distribution within interradicular bone. (d-e) Normalized frequency of maximum (d) and minimum (e) normal strains at different loading stages: 0–7 N, 7–15 N, 15–20 N. Average ± standard deviation of maximum and minimum strain values (%) are indicated. (f) Line profiles of maximum and minimum normal strains from coronal to apical (in z direction) in HF and SF groups indicated maximum variation at the coronal regions irrespective of SF or HF groups. Maximum strain values were recorded in the most coronal region of the interradicular bone.